Journal of Applied Electrochemistry (2006) 36:1187–1198
DOI 10.1007/s10800-006-9174-3

Electrooxidation of acetaldehyde on carbon-supported Pt, PtRu and Pt_3Sn and unsupported $PtRu_{0.2}$ catalysts: A quantitative DEMS study

H. WANG, Z. JUSYS and R.J. BEHM*
Department Surface Chemistry and Catalysis, University of Ulm, D-89069, Ulm, Germany
*(*author for correspondence E-mail: juergen.behm@uni-ulm.de)*

Received 30 August 2005; accepted in revised form 28 February 2006

Key words: acetaldehyde oxidation, CO_2 current efficiency, DEMS, selectivity, supported catalyst

Abstract

The oxidation of acetaldehyde on carbon supported Pt/Vulcan, PtRu/Vulcan and Pt_3Sn/Vulcan nanoparticle catalysts and, for comparison, on polycrystalline Pt and on an unsupported $PtRu_{0.2}$ catalyst, was investigated under continuous reaction and continuous electrolyte flow conditions, employing electrochemical and quantitative differential electrochemical mass spectroscopy (DEMS) measurements. Product distribution and the effects of reaction potential and reactant concentration were investigated by potentiodynamic and potentiostatic measurements. Reaction transients, following both the Faradaic current as well as the CO_2 related mass spectrometric intensity, revealed a very small current efficiency for CO_2 formation of a few percent for 0.1 M acetaldehyde bulk oxidation under steady-state conditions on all three catalysts, the dominant oxidation product being acetic acid. Pt alloy catalysts showed a higher activity than Pt/Vulcan at lower potential (0.51 V), but do not lead to a better selectivity for complete oxidation to CO_2. C–C bond breaking is rate limiting for complete oxidation at potentials with significant oxidation rates for all three catalysts. The data agree with a parallel pathway reaction mechanism, with formation and subsequent oxidation of CO_{ad} and $CH_{x,\,ad}$ species in the one pathway and partial oxidation to acetic acid in the other pathway, with the latter pathway being, by far, dominant under present reaction conditions.

1. Introduction

The oxidation of ethanol and other small organic molecules has attracted considerable interest because of their potential application in Direct Oxidation Fuel Cells [1–3]. Ethanol is particularly attractive in this respect because it can be easily produced in large quantities by fermentation of biomaterials and because of its lower toxicity compared, e.g., to methanol. A major problem, however, is the low activity of current catalysts for the complete oxidation of ethanol to CO_2, in particular for cleaving the C–C bond. As a result, incomplete oxidation of ethanol prevails and produces considerable amounts of acetaldehyde (e.g., [4]), which is toxic, polluting, and leads to a considerable loss of energy, since only two electrons are generated per ethanol molecule instead of 12 for complete oxidation of ethanol. Improving the further oxidation of acetaldehyde within the fuel cell is therefore of considerable interest for technical applications. Previous studies on acetaldehyde oxidation, however, are scarce and mostly deal with Pt electrodes [5–14]. First results on the performance of modified Pt and Pt alloy electrodes were reported in [6, 15]. In total, the studies identified two different reaction products for the oxidation of acetaldehyde, CO_2 and acetic acid [8, 9, 12–14], while ethane and methane were observed under reductive conditions [5]. CO_{ad} was identified as the only adsorbed reaction intermediate by IR [8–10, 12]. These results were explained by the proposal of two different, parallel reaction pathways for acetaldehyde oxidation, one leading via C–C bond breaking and CO_{ad} formation, to CO_2, possibly via weakly bound reaction intermediates, and the other one proceeding to CH_3COOH [9, 12, 15]. While this reaction scheme is accepted, the contributions of the two reaction pathways under different reaction conditions as well as further mechanistic details are still open. First results on the adsorption of acetaldehyde on carbon supported Pt/Vulcan catalysts [16] as well as on the adsorption and oxidation of ethanol [4, 17] on commercial Pt/Vulcan, PtRu/Vulcan, and Pt_3Sn/Vulcan catalysts have been previously reported.

Here we present results of a quantitative on-line differential electrochemical mass spectrometry (DEMS) study of acetaldehyde oxidation over commercial carbon supported platinum (Pt/Vulcan) and platinum alloy (PtRu/Vulcan and Pt_3Sn/Vulcan) catalysts (E-Tek, Inc.) under fuel cell relevant reaction conditions, including controlled mass transport and continuous reaction. For

comparison, we also performed measurements on an unsupported, Adams-type $PtRu_{0.2}$ catalyst and on a polycrystalline Pt electrode. The relevance of these results for the operation of Direct Oxidation Fuel Cells is briefly discussed.

2. Experimental

The DEMS set-up and the preparation of the carbon (Vulcan XC-72) supported Pt and Pt alloy catalyst thin-film electrodes as well as the physical properties of the catalysts have been described in previous publications [18–22]. In short, the DEMS set-up consists of two differentially pumped chambers, a Balzers QMS 112 quadrupole mass spectrometer, a Pine Instruments potentiostat and a computerized data acquisition system.

2.1. *Catalyst and thin-film electrodes*

The thin-film Pt/Vulcan, PtRu/Vulcan and Pt_3Sn/Vulcan catalyst (20 wt% metal loading, E-Tek, Inc., particle size: 3.7 ± 1.0, 2.1 ± 0.3, 3.8 ± 1.0 nm; dispersion: 26, 44, and 27%, respectively) and the $PtRu_{0.2}$ catalyst (Center for Solar Energy and Hydrogen Research (ZSW), Ulm, particle size: 5–6 nm, dispersion: 19%, preparation see [23, 24]) electrodes were prepared by pipetting and drying 20 μl of aqueous catalyst suspension (2 mg ml^{-1}) and then 20 μl Nafion aqueous solution on the central area of a mirror polished glassy carbon disk (Sigradur G from Hochtemperatur Werkstoffe GmbH, 9 mm in diameter), following procedures described earlier [18]. The catalyst thin film has a diameter of ca. 6 mm, resulting in a geometric surface area of 0.28 cm^2. Accordingly, the above procedure leads to a noble metal loading of 28 $\mu g\ cm^{-2}$ for the supported catalysts and of 140 $\mu g\ cm^{-2}$ for the unsupported PtRu catalyst. From the mean size of the nanoparticles, the metal surface area of the Pt/Vulcan, PtRu/Vulcan and Pt_3Sn/Vulcan electrodes was calculated to be 6.1, 13.6 and 7.1 cm^2 per 8 μg_{Me}, respectively, assuming spherical particle shapes. From the H-upd desorption charge on Pt/Vulcan and from the (mass spectrometric) CO stripping charge, we determined active surface areas of 5.9, 8.0 and 6.9 cm^2 per 8 μg_{Me} for the Pt/Vulcan, PtRu/Vulcan and Pt_3Sn/Vulcan electrodes, and 12.8 cm^2 for the unsupported PtRu catalyst per 40 μg_{Me}. These data, the metal loadings or the active surface areas determined from CO_{ad} stripping, can be used to convert the Faradaic currents given in all figures into mass specific currents or current densities, respectively.

The electrode was mounted into a dual thin-layer flow cell [25, 26] and pressed against a 50 μm thick spacer. This left an exposed area of 0.28 cm^2 and resulted in an electrolyte volume of ~5 μl at the working electrode, including the connecting capillaries. The electrolyte flow was driven by the hydrostatic pressure in the supply bottle(s) (flow rate about 10 $\mu l\ s^{-1}$), ensuring a fast transport of the species formed at the working electrode to the mass spectrometric compartment, where the volatile products were evaporated into the mass spectrometer (time constant ca. 1 s) through a porous membrane (Scimat, 60 μm thick, 50% porosity, 0.2 μm pore diameter).

2.2. *Electrochemical measurements*

Two Pt wires at the inlet and outlet of the thin-layer cell, connected through an external resistance (1 MΩ), were used as counter electrodes. A saturated calomel electrode (SCE), connected to the outlet of the DEMS cell via a Teflon capillary, served as reference electrode. All potentials, however, are quoted relative to that of the reversible hydrogen electrode (RHE).

The supporting electrolyte (0.5 M H_2SO_4) was prepared using Millipore Q water and ultrapure sulfuric acid (Merck, suprapur); acetaldehyde (p.a.) was obtained from Merck. Before the measurements the solutions were deaerated by high-purity Ar (MTI Gase, N6.0). All experiments were carried out at room temperature (23 ± 1 °C).

For the chronoamperometric measurements of the potential step transients, the potential was stepped from 0.06 or 0.26 V to the respective reaction potential, mostly 0.61 V. At the cathodic starting potential, the electrodes were equilibrated for ca. 10 min, to reach saturation of the adsorbate layer produced under these conditions (see [16]). The chronoamperometric measurements of the electrolyte exchange transients were performed by switching between two electrolyte supply bottles to the common inlet of the thin-layer flow cell, one with supporting electrolyte and the other one with a solution containing 0.1 M acetaldehyde. These experiments differ in so far as in the first case the catalyst is largely covered by acetaldehyde adsorbate before the potential step, while in the second case it is largely uncovered, except for adsorbed anions (all catalysts) or OH_{ad} species (PtRu/Vulcan and Pt_3Sn/Vulcan catalyst electrodes). The Faradaic and mass spectrometric ($m/z = 22$) current transients were measured for ca. 15 min at constant potential, after switching from pure supporting electrolyte to acetaldehyde containing solution, until reaching steady-state conditions. The amount of adsorbed decomposition products accumulated on the surface was determined by subsequent adsorbate stripping. The potential was stepped to 0.26 V at the end of the transient measurement, where desorption of the adsorbed acetaldehyde decomposition products is negligible [16]. Also, further adsorption during subsequent exchange of the acetaldehyde solution with pure supporting electrolyte (30 s after the potential step to 0.26 V) is largely inhibited. The potential scan for adsorbate stripping was followed by 3 potential cycles, with a low potential limit of 0.26 V to avoid reductive desorption of $CH_{x,ad}$. The relative coverage of adsorbed C1 species (CO_{ad} and $CH_{x,\ ad}$) compared to that of a

saturated CO adlayer on the respective catalyst was quantified by comparison with the amount of CO_2 formed after oxidation of a saturated CO adlayer produced upon adsorption from a CO saturated electrolyte. CO_2 formation was integrated over the stripping scan plus the subsequent three potential cycles.

2.3. *DEMS measurements*

Because of the high intensity of acetaldehyde on the $m/z = 44$ signal typical for CO_2, we followed CO_2 formation in the acetaldehyde oxidation by monitoring the $m/z = 22$ signal (intensity for CO_2: 2.8% of the $m/z = 44$ signal [4]).

The current efficiency of the reaction product CO_2, $A_q(CO_2)$ or $A_i(CO_2)$, was calculated from the $m/z = 22$ charge (current) using the following equations:

$$A_q(CO_2) = 5Q_i/(K_{22}^* Q_f) \quad \text{or} \quad A_i(CO_2) = 5I_i/(K_{22}^* I_f) \tag{1}$$

where Q_f and I_f are the Faraday charge and Faraday current during acetaldehyde oxidation, respectively, and Q_i and I_i denote the corresponding mass spectrometric charge/current of the $m/z = 22$ signal. K^* denotes the calibration constant of the DEMS set-up, which was determined by calibration measurements using CO bulk oxidation for acetaldehyde bulk oxidation [4, 17, 27, 28]. The factor 5 accounts for the number of electrons needed for formation of one CO_2 molecule from acetaldehyde.

3. Results and discussion

3.1. *Acetaldehyde oxidation and reduction on polycrystalline Pt and Pt/Vulcan catalysts*

The cyclic voltammograms (CVs) and the corresponding mass spectrometric cyclic voltammograms (MSCVs) for acetaldehyde oxidation on polycrystalline Pt (Figure 1a and b) and on the Pt/Vulcan electrode (Figure 1c, d) are shown in Figure 1. The base CVs in 0.5 M H_2SO_4 solution (dotted lines in Figure 1a and c) are identical to those reported earlier for these electrodes [21, 29]. The general behavior of acetaldehyde oxidation on these electrodes is very similar. In the positive-going scan, the CVs exhibit two characteristic peaks with maxima at 0.9 and 1.25 V, respectively, and a shoulder in the lower potential peak at 0.7 V (for discussion see below). For the Pt/Vulcan electrode, the CV was limited to an upper potential of 1.16 V to avoid oxidation of the carbon support. In the negative-going scan, the high potential peak is practically absent on the Pt electrode and the low potential peak is shifted negatively, with two distinct maxima at 0.73 and 0.64 V for polycrystalline Pt and at 0.74 and 0.60 V for the Pt/Vulcan catalyst. These general characteristics agree with previous reports for acetaldehyde oxidation on Pt [5, 7–12, 14].

Comparison with the MSCVs for CO_2 ($m/z = 22$, Figure 1b and d) shows that the main maximum (0.9 V) of the low potential peak and the high potential Faradaic current peak at 1.25 V are not correlated with CO_2 formation and hence must be due to the formation of acetic acid (see below). CO_2 formation is only observed in a peak corresponding to the low potential shoulder of the first peak in the CV, starting at 0.5 V and passing through a maximum at 0.78 V. We suggest that the shoulder in the low potential peak of the positive-going scan is caused by oxidation of CO_{ad} formed by acetaldehyde decomposition at lower potentials. In the negative-going scan, CO_2 formation is almost completely inhibited. The shape and total charge density in the CO_2 formation peak (positive-going scan) resembles that obtained for acetaldehyde adsorbate oxidation on Pt/Vulcan [16], which implies that CO_2 is mainly formed via oxidation of adsorbed species resulting from decomposition of acetaldehyde at low potentials, i.e., in the low potential range of the positive-going and the preceding negative-going scan. Similar conclusions have been reported also by Rodriguèz et al. [12]. Based on the number of electrons generated per CO_2 molecule (around 2) [16] and by comparison with previous IR data [8–10, 12] these decomposition products are at least predominantly CO_{ad}.

Despite of diligent testing we found no potential dependent signals related to volatile reaction products other than CO_2 and small amounts of methane/ethane under reductive conditions (see below). Considering the low amount of CO_2 formation and the low volatility of acetic acid at low concentrations (product concentrations are less than 1 mM), the main reaction product for acetaldehyde oxidation must be acetic acid, which was found to be stable against oxidation at room temperature.

Assuming that CO_2 formation from acetaldehyde generates five electrons per CO_2 product molecule, the Faradaic current contribution arising from the CO_{ad} pathway was calculated, which is included as a thick solid line in Figure 1a and c. CO_{ad} and $CH_{x,\ ad}$ formation are likely to take place at lower potentials in the CVs, therefore the calculated CO_2 contribution to the Faradaic current during CO_2 formation should be taken as an upper limit. (This does not affect the CO_2 current efficiencies calculated over an entire potential cycle.) These traces clearly show that also for those peaks in the Faradaic current where CO_2 formation is observed, this is a minor contribution to the total Faradaic current. Furthermore, these results also indicate that acetaldehyde can only be oxidized at potentials above the onset for acetaldehyde adsorbate oxidation, and that at lower potentials the surface is completely blocked for acetaldehyde bulk oxidation. The Faradaic current peak at high potentials, in the range around 1.25 V, illustrates that acetaldehyde can also be oxidized to acetic acid on an oxidized Pt surface at these potentials, which is inhibited at lower potentials (around

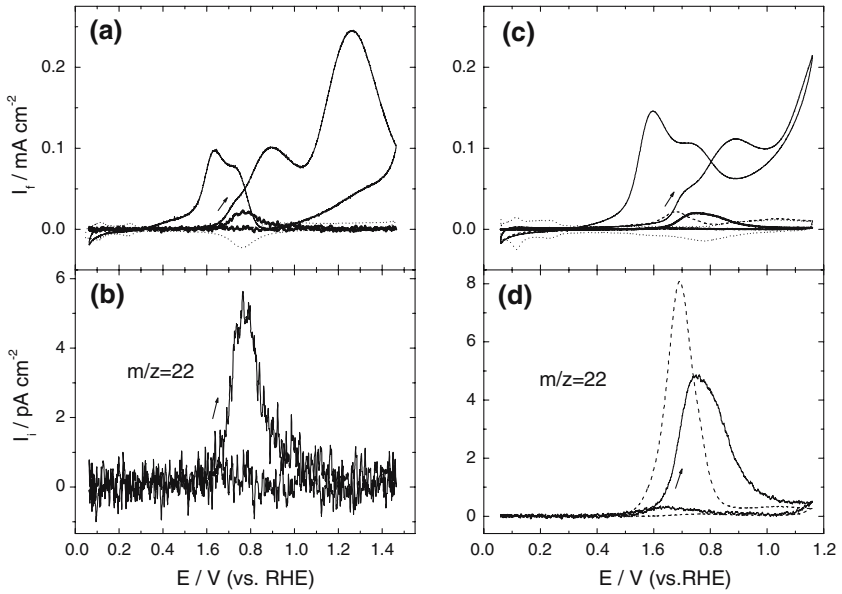

Fig. 1. Simultaneously recorded CVs (a, c) and m/z = 22 MSCVs (b, d) for the oxidation of acetaldehyde in 0.1 M CH_3CHO + 0.5 M H_2SO_4 solution on a polycrystalline Pt electrode (a, b) and on a Pt/Vulcan electrode (c, d) (full line). Dotted line (.....) indicates the base CVs of the polycrystalline Pt and Pt/Vulcan electrodes in 0.5 M H_2SO_4 solution, respectively. Thick solid line (—) shows the calculated contribution of CO_2 formation to the Faradaic current signal (a, c). For comparison, the oxidative stripping of acetaldehyde adsorbate formed at 0.31 V is also shown by dashed line (- - - -). Scan rate: 10 mV s^{-1}.

1.0 V), where Pt oxidation has started [29], but the acetaldehyde oxidation rate passes through a minimum.

The detection of methane and ethane formation in the H-upd region, which have been observed for acetaldehyde adsorbate stripping in this potential region [7, 14, 16] and have also been reported for acetaldehyde bulk reduction [5], is hindered by the background intensity on the m/z = 15 and 30 signals arising from acetaldehyde fragmentation. Therefore, similar experiments were performed at a lower acetaldehyde concentration (0.01 M) to reduce the background intensity on these signals (Figure 2), with a negative potential limit of 0 V. Under these conditions the Faradaic current increases at the most cathodic potentials, which is associated with methane and ethane formation. By comparison with data obtained for acetaldehyde adsorbate stripping in inert supporting electrolyte [16], it follows that methane formation arises from the reduction of adsorbed CH_x species, which are formed upon acetaldehyde decomposition in the low potential region of the CV, while ethane formation originates from bulk reduction of acetaldehyde (see also Figure 3). The negative peak in the m/z = 15 signal at about 0.5 V, in the negative-going scan, is accompanied by a decrease in acetaldehyde concentration due to oxidation to acetic acid at this potential (see Figure 2(a)). The much lower decrease of the acetaldehyde concentration in the positive-going scan supports the conclusion that, in that scan, the Faradaic current results mostly from adsorbate oxidation and Pt oxidation.

Methane and ethane formation during acetaldehyde reduction (see Figure 2c and d) were further investigated by a potential step experiment, stepping the potential from 0.31 V to 0.06 V (Figure 3). The evolution of the m/z = 15 peak shows a pronounced spike right after the potential step, which corresponds to methane formation. This spike, which appears also in the Faradaic

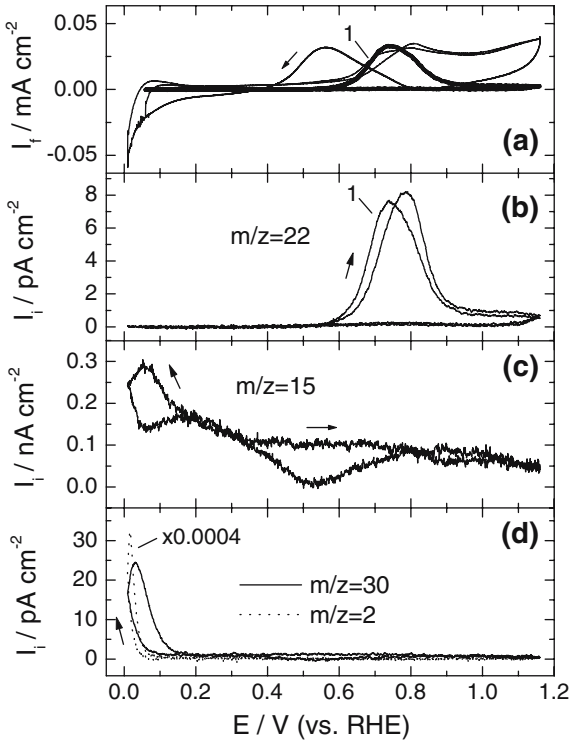

Fig. 2. Simultaneously recorded CVs (a) and MSCVs for m/z = 22 (b), m/z = 15 (c), and m/z = 30 and m/z = 2 (d) on a Pt/Vulcan electrode in 0.01 M CH_3CHO + 0.5 M H_2SO_4 solution. Thick solid line (—) shows the calculated contribution of CO_2 formation to the Faradaic current signal (a). Scan rate: 10 mV s^{-1}. The numbers in the figure indicate the times of potential cycles.

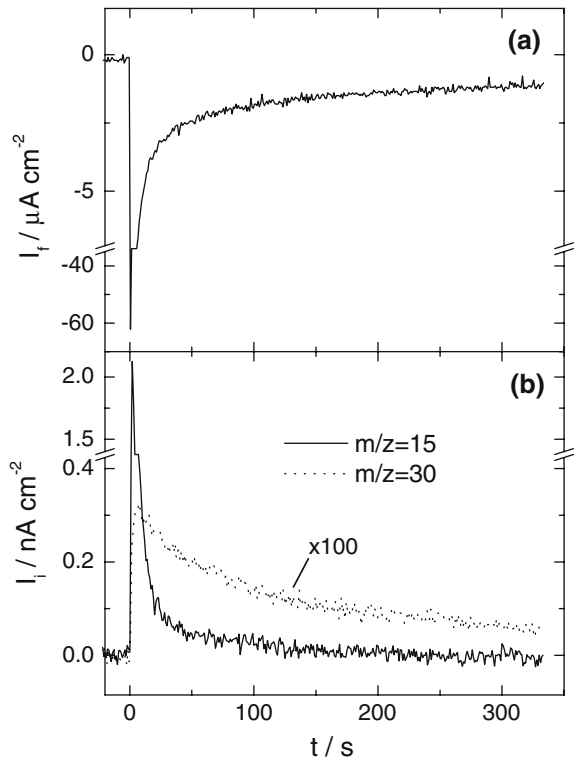

Fig. 3. Simultaneously recorded Faradaic current (a) and ion current (m/z = 15 and m/z = 30) (b) transients after a potential step from 0.31 to 0.06 V on a Pt/Vulcan electrode in 0.01 M CH_3CHO + 0.5 M H_2SO_4 solution.

current signal (in addition to capacitive charging), however, decreases quickly to almost zero within 2 minutes. In contrast, ethane formation (m/z = 30), which also starts after the potential step, does not exhibit the sharp initial spike, but instead passes through a shallow maximum and then decreases slowly, being still active after 10 min. We conclude that at 0.06 V, methane is formed by hydrogenation of adsorbed acetaldehyde decomposition products, which were produced upon interaction with the Pt/Vulcan catalyst at 0.31 V, while ethane is produced via bulk reduction of acetaldehyde (see also [14, 16]).

For the lower acetaldehyde concentration, the CO_2 related signal in Figure 2(b) resembles much more the Faradaic current signal than at the higher concentration, indicating that the contribution from CO_2 formation to the Faradaic current signal is much more pronounced than at the higher concentration in Figure 1. This is illustrated also by the partial reaction current calculated for CO_2 formation calculated as described above. The peak in the negative-going scan is again solely due to acetic acid formation as no CO_2 formation is observed. Comparing the first and the second positive-going scan in the CV and MSCV (m/z = 22), the onset and the peak maximum for CO_2 formation are shifted positively (peak shift from 0.73 to 0.78 V) with decreasing lower potential limit, which is attributed to the presence of reduced C2 adspecies. These must have been produced at lower potentials and were not been completely removed by reductive stripping [16]. A similar behavior was observed for ethanol oxidation on a Pt/Vulcan electrode [4].

The average current efficiencies for CO_2 formation, integrated over a complete potential cycle (Figure 1), are 4% for the polycrystalline Pt electrode and 5% for the Pt/Vulcan electrode, respectively (Table 1 and Figure 1). The results apparently depend little on the (active) surface area of the electrode or the catalyst layer, which is about ten times higher for the Pt/Vulcan catalyst than for the pc Pt electrode. This supports the above hypothesis that CO_2 formation occurs largely by oxidation of acetaldehyde adsorbate (CO_{ad}) that has been formed at low potentials in the potential scan, since adsorbate formation should be independent of surface roughness, at least in the absence of pronounced diffusion limitations, opposite to the findings for methanol oxidation [30, 31]. Since acetic acid cannot be further oxidized at ambient temperature, the increase in the loading or the roughness factor does not enhance the chance for the further oxidation of acetic acid, and therefore, the current efficiency for CO_2 formation during acetaldehyde oxidation depends little on the catalyst loading or the roughness factor.

Similar conclusions can also be drawn from the effect of acetaldehyde concentration on the oxidation behavior (Figure 2). In 0.01 M acetaldehyde solution reduces the Faradaic current by about a factor of four, while the amount and characteristics of CO_2 formation remain

Table 1. Comparison of the currents and CO_2 current efficiencies for acetaldehyde oxidation on the Pt/Vulcan, PtRu/Vulcan, Pt_3Sn/Vulcan and $PtRu_{0.2}$ catalyst electrodes

	Pt/Vulcan	PtRu/Vulcan	Pt_3Sn/Vulcan
A_q (0.1 M[c])	5% (0.2–1.16 V)	11% (0.2–0.81 V)	6% (0.2–0.61 V)
A_q (0.01 M[c])	23% (0.2–1.16 V)	22% (0.2–0.81 V)	Not meas.
A_i (0.61 V)	4–7%	1%	2%
I (0.61 V) potential step	0.011 mA cm^{-2}	0.008 mA cm^{-2}	0.005 mA cm^{-2}
I (0.51 V) electrolyte exchange	0.001 mA cm^{-2}	0.007 mA cm^{-2}	0.006 mA cm^{-2}
I (0.61 V) electrolyte exchange	0.012 mA cm^{-2}	0.008 mA cm^{-2}	0.012 mA cm^{-2}

A_q: average current efficiency for CO_2 obtained by integration over one complete cycle (potential scan range is given in brackets), A_i, I: steady-state current efficiencies (A_i) and steady-state currents (I) for acetaldehyde oxidation at 0.61 V in 0.1 M acetaldehyde solution after 10 min. reaction time (potential step measurements), and steady-state currents I (0.51 V) and I (0.61 V), respectively, for acetaldehyde oxidation at 0.51 and 0.61 V in 0.1 M acetaldehyde solution after 10 min reaction time measured in electrolyte exchange transients.

largely unchanged. Hence, the current efficiency for CO_2 formation increases to over 20% (Table 1).

Potential step transients recorded on the Pt/Vulcan electrode upon stepping the potential from 0.06 to 0.61 V or from 0.26 to 0.61 V, respectively, are shown in Figure 4 (a–c). In both cases, the initial Faradaic currents and CO_2 related MS signals are significantly higher right after the potential step than under steady state conditions, which are approximately reached after 15 min. Acetaldehyde can already be adsorbed on Pt at 0.06 V [16]. The initial spike in Faradaic current and CO_2 formation, after stepping from 0.06 to 0.61 V (full line, Figure 4a), is therefore attributed to the oxidation of adsorbed species formed at 0.06 V. The subsequent slow increase in Faradaic current is correlated with a slow decrease in CO_2 formation, indicating that the coverage of adsorbed acetaldehyde decomposition products, mainly CO_{ad}, decreases slowly. This is most simply explained by a slow equilibration between the low CO_{ad} formation rate at 0.61 V and the equally slow CO_{ad} oxidation rate at this potential. Under steady-state conditions, the Faradaic current density and the current efficiency for CO_2 formation are around 0.011 mA cm^{-2} and 7%, respectively, i.e., the current efficiency is higher than the average current efficiency for CO_2 formation determined in the CVs (Table 1), but still unsatisfactory for practical applications.

Stepping the potential from 0.26 to 0.61 V (Figure 4(a)), the current passes through an initial spike and then increases again, until it passes through a smooth maximum after about 65 s, and then decays again. The $m/z = 22$ signal also exhibits the initial spike, followed by an exponential decay. The higher Faradaic current after stepping from 0.26 V, which even after 15 min is about 20% higher than that obtained after stepping from 0.06 V, is due to fewer C2 adspecies compared to that for 0.06 V starting potential [16]. The higher Faradaic current (0.016 mA cm^{-2}) and the lower CO_2 formation rate, after stepping from 0.26 V, result in a lower CO_2 current efficiency of around 4% compared to 7% after stepping from 0.06 V (Figure 4(c)). It should be noted that this is mainly due to a lower rate for acetic acid formation in the latter case, not to a higher absolute rate for CO_2 formation. In both cases, however, the current efficiency of CO_2 is very low, making incomplete oxidation to acetic acid the by far dominating reaction pathway for acetaldehyde oxidation on Pt/Vulcan under present reaction conditions. The difference between the Faradaic current and the CO_2 formation rates for different starting potentials also indicates that steady-state conditions, which should be independent of the initial potential, have not yet been reached.

Corresponding Faradaic and mass spectrometric current density ($m/z = 22$) transients, recorded after switching from pure supporting electrolyte to 0.1 M acetaldehyde containing solution, are shown in Figure 5(a, b). The Faradaic current rises steeply upon admission of acetaldehyde solution, passes through an initial maximum and then decays in roughly an exponential way towards its steady-state value. Both the initial maximum and the steady-state current density are significantly higher for 0.61 V than for 0.51 V reaction potential. The mass spectrometric current of $m/z = 22$ (Figure 5(b)) also increases steeply upon admission of acetaldehyde solution. Most of this increase, however, is related to an increase in background intensity, due to fragmentation of acetaldehyde. For 0.61 V reaction potential, the mass spectrometric current of $m/z = 22$

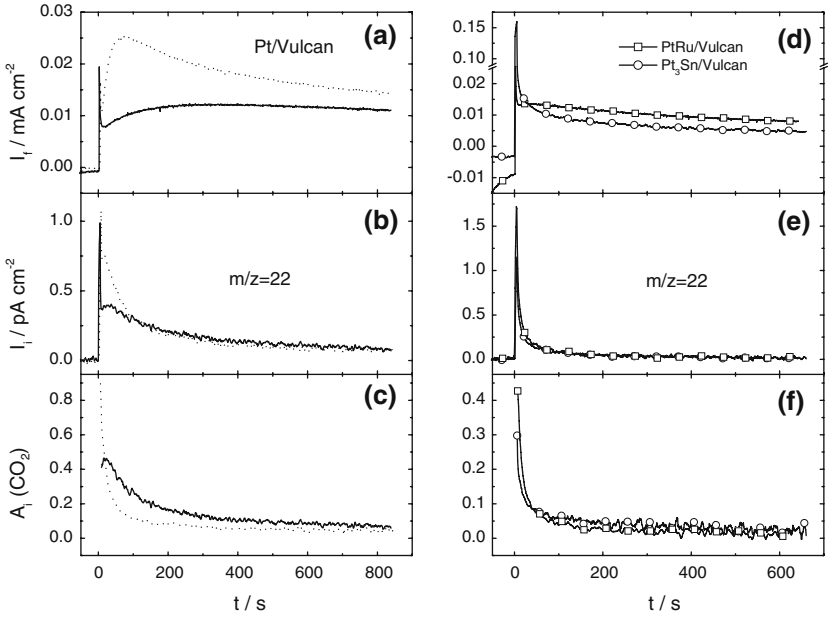

Fig. 4. Simultaneously recorded Faradaic current (a, d) and $m/z = 22$ ion current transients (b, e) after a potential step from 0.06 (—,–□–, – ○–) and from 0.26 to 0.61 V (.....) on a Pt/Vulcan, PtRu/Vulcan and Pt_3Sn/Vulcan electrodes in 0.1 M CH_3CHO + 0.5 M H_2SO_4 solution. Figure 4c and f shows the current efficiency for CO_2 formation.

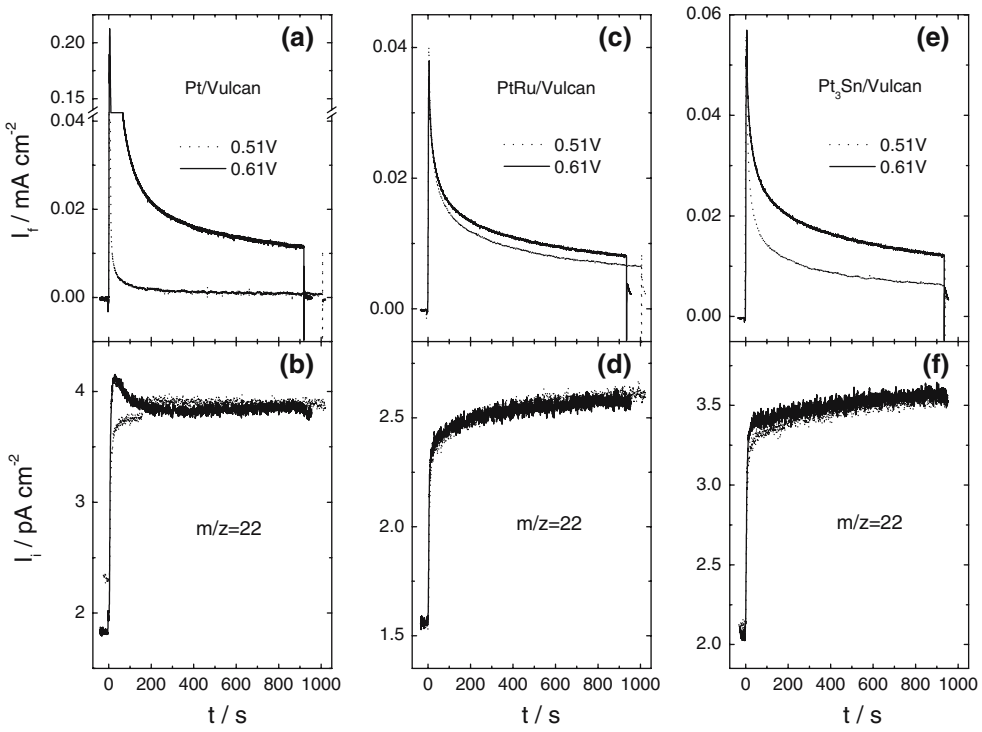

Fig. 5. Faradaic current (a, c, e) and $m/z = 22$ mass spectrometric current transients (b, d, f) on Pt/Vulcan, PtRu/Vulcan and Pt_3Sn/Vulcan electrodes at 0.51 V (dotted lines) and 0.61 V (full lines) reaction potential upon changing from 0.5 M H_2SO_4 solution to 0.1 M acetaldehyde + 0.5 M H_2SO_4 solution.

exhibits a maximum in the beginning of the transient, which we attribute to CO_2 formation superposed on the background increase. After 2 min, the mass signal remains constant. For adsorption/reaction at 0.51 V, we found no maximum of the mass signal, and the signal steadily approaches its steady-state value. The absence of an initial maximum in the $m/z = 22$ signal at 0.51 V can be explained by the much smaller rate for CO_{ad} oxidation at this potential compared to 0.61 V (Figure 5b).

Stepping the potential to 0.26 V (Figure 5(a, b)), shows only a negligible change of the mass spectrometric signal, at least on this sensitivity scale. Similar to our findings in potential step measurements, acetaldehyde oxidation mainly produces acetic acid under steady-state conditions, as found also in the potential step measurements. The Faradaic current density during acetaldehyde oxidation of 0.001 mA cm^{-2} at 0.51 V and 0.012 mA cm^{-2} at 0.61 V (Table 1), respectively, is close to the values obtained in the potential step measurements.

Figure 6(a, b) illustrates the acetaldehyde adsorbate stripping behavior after electrolyte exchange, according to the procedure described in Section 2. As previously shown [16], acetaldehyde dissociates to CO_{ad} and $CH_{x,\,ad}$ upon adsorption. During adsorbate stripping, CO_{ad} is oxidized in the low potential peak ($\leq$0.85 V); $CH_{x,ad}$ is more difficult to oxidize than CO_{ad} and reacts mainly at potentials positive of 0.85 V. The relatively high intensity in the latter potential regime, related to CO_2 formation from $CH_{x,\,ad}$ and possibly also trace amounts of adsorbed C2 species, can be explained by the higher adsorption potential compared to the adsorption transients (0.06–0.36 V) shown in [16]. For adsorption under reactive conditions, where CO_{ad} oxidation is already possible, at least at a very low rate, the slow removal of CO_{ad} allows the accumulation of higher coverages of $CH_{x,\,ad}$ species compared to adsorption at lower potentials. This is even more pronounced upon adsorption at 0.61 V. The total coverage of C1 species, relative to that of a saturated CO adlayer formed from CO saturated solution, is ca. 0.6 at both potentials, i.e., the increase in $CH_{x,\,ad}$ coverage at higher reaction potential is compensated by a decrease in CO_{ad} coverage. The steady-state acetaldehyde oxidation rate on the remaining free surface area, however, increases significantly from 0.51 to 0.61 V, reflecting a higher activity per free surface site under the latter conditions.

3.2. *Acetaldehyde oxidation on PtRu/Vulcan and $PtRu_{0.2}$(Adams) catalysts*

A set of measurements similar to those presented in Section 3.1 was also performed on the carbon supported PtRu/Vulcan catalyst (Figures 4–8), and, partly, on an unsupported $PtRu_{0.2}$ Adams-type (Figure 9) catalyst. In order to avoid Ru leaching, the positive potential limit was lowered to 0.8 V in these scans.

The base CV of the PtRu/Vulcan (dashed line, Figure 7(a)) exhibits the structureless shape typical for PtRu electrodes [32–35]. The oxidation of acetaldehyde resembles that on Pt/Vulcan with the following differences: Acetaldehyde oxidation starts at 0.3 V, which is

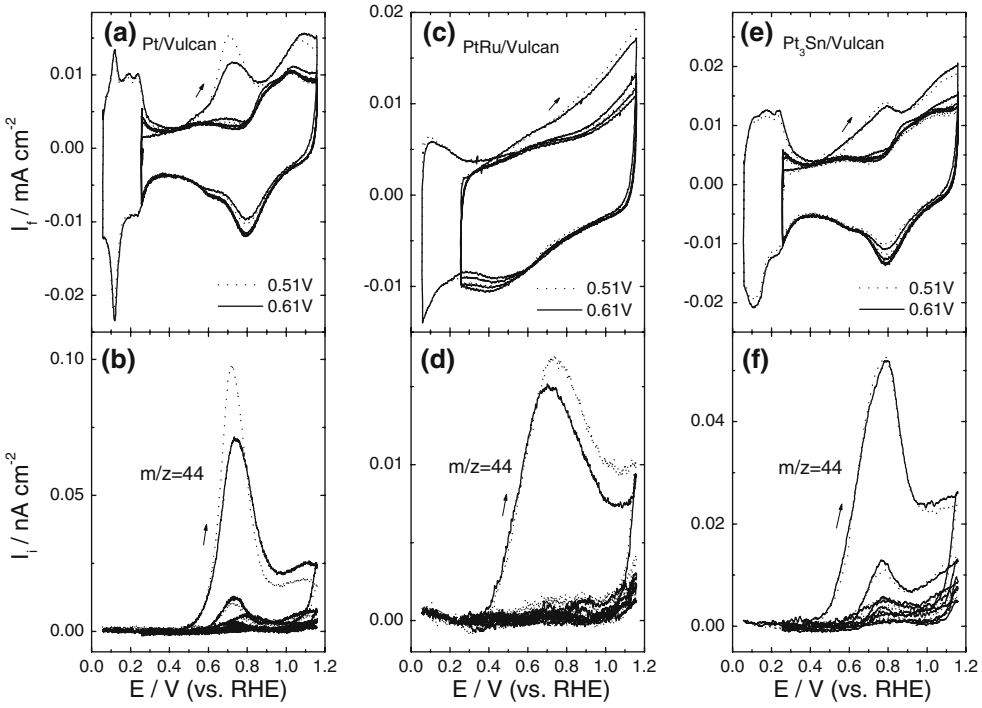

Fig. 6. Simultaneously recorded CVs (a, c, e) and MSCVs of m/z = 44 (b, d, f) for acetaldehyde adsorbate stripping after 15 min acetaldehyde adsorption/oxidation on Pt/Vulcan, PtRu/Vulcan and Pt_3Sn/Vulcan electrodes (see Figure 5) at 0.51 V (dotted lines) and 0.61 V (full lines). Scan rate: 10 mV s^{-1}.

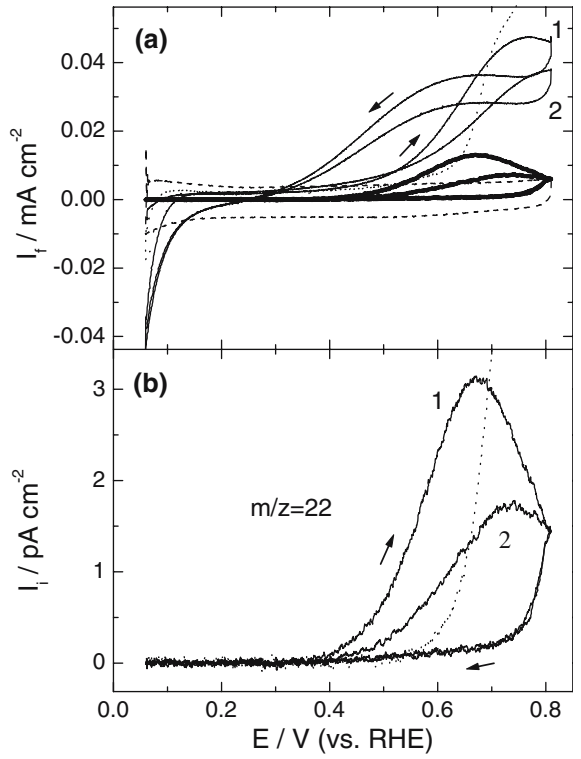

Fig. 7. Simultaneously recorded CVs (a) and MSCVs of m/z = 22 (b) for the oxidation of acetaldehyde on a PtRu/Vulcan electrode in 0.1 M CH_3CHO + 0.5 M H_2SO_4 solution. For comparison the oxidation of acetaldehyde on Pt/Vulcan is also included (.....). Thick solid (—) and dashed (- - - -) lines (a) indicate the contribution of CO_2 formation to the Faradaic current and the base CV of PtRu/Vulcan in 0.5 M H_2SO_4 solution, respectively. Scan rate: 10 mV s^{-1}. The numbers in the figure indicate the times of potential cycles.

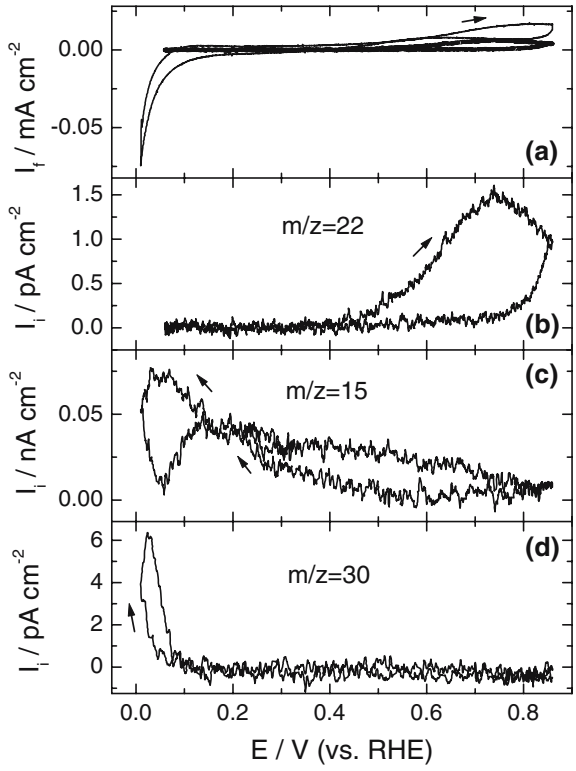

Fig. 8. Simultaneously recorded CVs (a) and MSCVs m/z = 22 (b), m/z = 15 (c) and m/z = 30 as well as m/z = 2 (d) on a PtRu/Vulcan electrode in 0.01 M CH_3CHO + 0.5 M H_2SO_4 solution. Thick solid line (—) shows the calculated contribution of CO_2 formation to the Faradaic current signal (a). Scan rate: 10 mV s^{-1}.

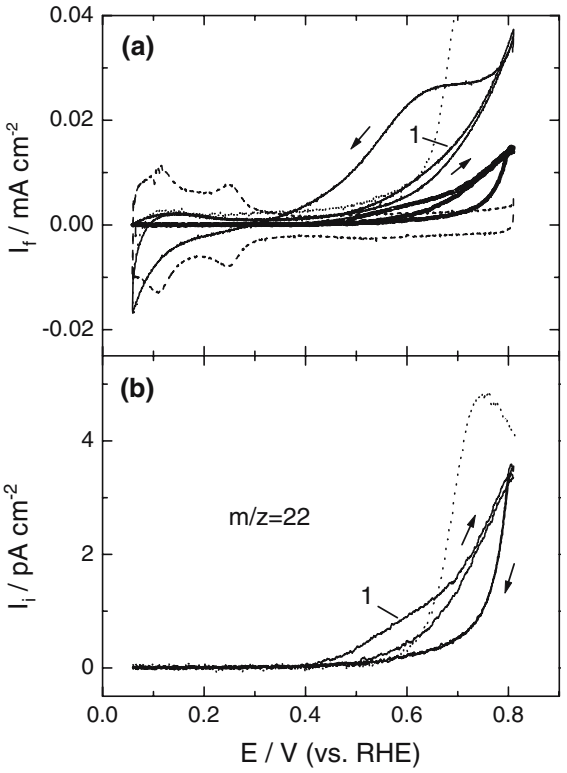

Fig. 9. Simultaneously recorded CVs (a) and MSCVs $m/z = 22$ (b) for the oxidation of acetaldehyde on a $PtRu_{0.2}$ Adams-type electrode in 0.1 M CH_3CHO + 0.5 M H_2SO_4 solution. For comparison the oxidation of acetaldehyde on Pt/Vulcan is also included (.....). Thick solid (—) and dashed (- - - -) lines (a) indicate the contribution of CO_2 formation to the Faradaic current and the base CV of $PtRu_{0.2}$ in 0.5 M H_2SO_4 solution, respectively. Scan rate: 10 mV s^{-1}. The numbers in the figure indicate the times of potential cycles.

more than 200 mV more negative compared to Pt/Vulcan, and then increases steadily up to the positive limit of 0.8 V. In the negative-going scan, the Faradaic current remains constant down to 0.6 V and then decreases steadily, followed by an increasing reduction current at potentials negative of 0.23 V. The cathodic current in the H-upd regime is significantly more pronounced than for Pt/Vulcan (Figure 1(c)), which based on MS results (not shown here), is due to an enhanced H_2 evolution.

CO_2 formation starts at 0.4 V, more than 100 mV more negatively compared to Pt/Vulcan (Figure 1(d)), but the negative shift in Faradaic current is much more pronounced than that for CO_2 formation. This means that the down-shift in the onset for acetaldehyde oxidation is caused by a shift in the onset for incomplete oxidation to acetic acid. Hence, the acetaldehyde adsorbate coverage reached in the low potential range is sufficient to inhibit further C–C bond breaking and CO_{ad} formation, but is not sufficient to block partial oxidation of acetaldehyde to acetic acid. This is similar to the behavior observed for ethanol and ethylene glycol oxidation on PtRu/Vulcan [17, 22]. The increase in the acetaldehyde oxidation current is, however, much less pronounced than on Pt/Vulcan (see dotted line in Figure 7(a)), so that for potentials > 0.67 V the latter catalyst is more active for acetaldehyde oxidation than PtRu/Vulcan. Finally, for PtRu/Vulcan, no CO_2 formation is observed during the negative-going scan, which supports the assumption stated above that also on this catalyst, CO_2 formation is related to the oxidation of CO_{ad} which is produced in the low potential regime, but does not result from acetaldehyde bulk oxidation.

The average current efficiency for CO_2 formation in one potential cycle, calculated from these data, is about 11% (see Table 1). Similar as for the Pt/Vulcan electrode, we calculated the contribution of CO_2 formation to the total Faradaic current, which is included as the thick solid line in Figure 7(a). Again, the contribution of CO_2 formation to the total Faradaic current is small in the high potential region of the positive-going scan; the majority Faradaic current is caused by acetaldehyde oxidation to acetic acid.

Measurements in 0.01 M acetaldehyde solution (Figure 8) show a much more pronounced contribution of CO_2 formation than at the higher concentration, reaching 22% over a full potential cycle (for the integration, we did not include the signal in the H_2 evolution range) (Table 1). The same trend is illustrated by the contribution of the CO_2 formation current to the total Faradaic current (thick solid line in Figure 8(a)). Methane and ethane formation occur in the same potential regions as on the Pt electrode (Figure 8c and d); their amount, however, is significantly reduced compared to that on the Pt/Vulcan catalyst.

Steady-state Faradaic (Figure 4(d)) and mass spectrometric currents ($m/z = 22$, Figure 4e) as well as the CO_2 current efficiency (Figure 4f) for acetaldehyde oxidation on the PtRu electrode, measured as transients upon stepping the potential from 0.06 to 0.61 V, are shown in Figure 4. The general behavior of these transients is similar to those recorded on Pt/Vulcan. The Faradaic current decays rapidly to a value of around 0.01 mA cm^{-2}. After 10 min (quasi steady-state), the current efficiency is about 1%, which is significantly less than the average CO_2 current efficiency obtained in the potentiodynamic measurements, but also much less than for Pt/Vulcan.

Faradaic current transients and $m/z = 22$ mass spectrometric current transients, recorded on PtRu/Vulcan after switching from pure supporting electrolyte to 0.1 M acetaldehyde containing solution, are shown in Figure 5c and d. Similarly to Pt/Vulcan, the Faradaic current also rises steeply upon admission of acetaldehyde solution, passes through a maximum and then decays (peak current density 0.045 mA cm^{-2} for both potentials, 0.51 and 0.61 V). After 15 min, the Faradaic current density for acetaldehyde oxidation has reached quasi steady-state values of 0.007 mA cm^{-2} at 0.51 V and 0.008 mA cm^{-2} at 0.61 V, respectively. While the value at 0.61 V is of similar order of magnitude as that on Pt/Vulcan, the current density at 0.51 V is significantly higher on PtRu/Vulcan than on Pt/Vulcan, which is attributable to the higher activity for CO_{ad} oxidation of the latter catalyst under these conditions.

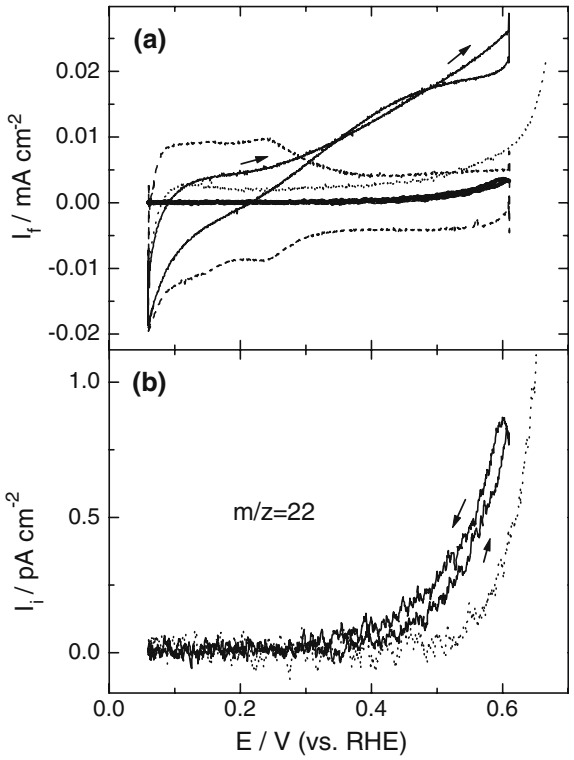

Fig. 10. Simultaneously recorded CVs (a) and MSCVs $m/z = 22$ (b) for the oxidation of acetaldehyde on a Pt_3Sn/Vulcan electrode in 0.1 M CH_3CHO + 0.5 M H_2SO_4 solution. For comparison the oxidation of acetaldehyde on Pt/Vulcan is also included (.....). Thick solid (—) and dashed (- - - -) lines (a) indicate the contribution of CO_2 formation to the Faradaic current and the base CV of Pt_3Sn/Vulcan in 0.5 M H_2SO_4 solution, respectively. Scan rate: 10 mV s^{-1}.

The $m/z = 22$ mass spectrometric current (Figure 5d) behaves similarly to that on Pt/Vulcan at 0.51 V at both potentials, increasing steeply upon admission of acetaldehyde solution, and then approaching the steady-state value without passing through an initial maximum. No change in $m/z = 22$ signal is observed when stepping the potential to 0.26 V after 15 min. This indicates that acetaldehyde oxidation on PtRu/Vulcan produces mainly acetic acid at steady-state, as found from analogous potential step experiments (Figure 4d–f). For PtRu/Vulcan, the rate and amount of CO_{ad} formation is significantly smaller than on Pt/Vulcan, as indicated by the MSCVs in Figures 1d and 7b, so that even the higher CO_{ad} oxidation rates on PtRu/Vulcan do not lead to a current spike for CO_2 formation that can be resolved in the pronounced increase of background intensity.

Figure 6c and d illustrates the acetaldehyde adsorbate stripping behavior. In this case the Faradaic current increases steadily from 0.26 V on, with a slightly higher value after reaction at 0.51 V than after reaction at 0.61 V. The positive potential limit (1.16 V) was rather high to ensure complete oxidation of adsorbed species, which will, of course, also lead to Ru oxidation and leaching. Hence, a new thin-film electrode was prepared for each experiment. Acetaldehyde adsorbate stripping on PtRu/Vulcan also exhibits two oxidation regions, with significant intensity for the high potential peak, where the high-potential CO_2 signal is assigned to the oxidation of $CH_{x,ad}$ and trace amounts of C2 adspecies, and the low potential signal to oxidation of CO_{ad} and partly also $CH_{x,ad}$. The relative coverage of C1 species, is ca. 0.2 for both potentials. This is much lower than the coverage of the steady-state adsorbate layer on Pt/Vulcan (Section 3.1), which suggests a lower acetaldehyde dissociation rate and higher CO_{ad} and $CH_{x,ad}$ oxidation rates on PtRu/Vulcan compared to Pt/Vulcan.

The influence of the catalyst (surface) composition on the acetaldehyde oxidation reaction was evaluated by performing comparative potentiodynamic measurements on an unsupported, Pt-rich $PtRu_{0.2}$ Adams-type catalyst electrode (Figure 9). The base CV recorded on the catalyst electrode (dashed line, Figure 9a) shows pronounced H-upd adsorption and desorption features, which agree well with a Pt-rich surface composition. The CVs and MSCVs recorded in acetaldehyde solution largely resemble those obtained for the PtRu/Vulcan electrode. CO_2 formation starts at 0.45 V in the positive-going scan, i.e., 50 mV more positive compared to PtRu/Vulcan, but still more than 50 mV more negative than on Pt/Vulcan. (Note that in the first positive-going scan CO_2 formation starts at 0.4 V.) Similarly to Pt/Vulcan, partial oxidation to acetic acid is not possible on the adsorbate covered catalyst surface. The average current efficiency for CO_2 formation over a full potential cycle of around 20% (Table 1) is significantly higher than for both the Pt/Vulcan and PtRu/Vulcan electrodes.

3.3. *Acetaldehyde oxidation on Pt_3Sn/Vulcan catalyst*

Similar potentiodynamic (Figure 10) and transient potentiostatic measurements (Figures 4(d–f), 5(e, f)) as discussed in the preceding sections for Pt/Vulcan and PtRu/Vulcan, were also carried out on a carbon supported Pt_3Sn/Vulcan catalyst. To avoid Sn dissolution the positive potential limit was further reduced to 0.6 V.

The base CV of Pt_3Sn/Vulcan (dashed line in Figure 10(a)) shows that the H-upd peaks are almost completely suppressed, in good agreement with previous work [36, 37]. In the positive-going scan, CO_2 formation starts at 0.35 V, i.e., 150 mV more negative than on Pt/Vulcan. Acetaldehyde oxidation starts at around 0.2 V, which is 300 mV negative of the onset of acetaldehyde oxidation on Pt/Vulcan. The acetaldehyde oxidation current is higher than that on Pt/Vulcan over the entire potential range up to 0.6 V. In the negative-going scan the oxidation current decays only slowly down to 0.45 V. The cathodic current at potentials < 0.2 V is mainly attributable to the formation of methane and ethane, and, at more cathodic potentials, increasingly to H_2 evolution, as discussed for the PtRu/Vulcan catalyst.

The average current efficiency for CO_2 formation, integrated over a full potential cycle, is around 6% (Table 1), close to that on the Pt/Vulcan catalyst, but lower than for the PtRu/Vulcan catalyst. Hence, on Pt_3Sn/Vulcan acetaldehyde oxidation is also dominated by incomplete oxidation to acetic acid. The potential

dependent contribution of CO_2 formation to the total Faradaic current is illustrated by the thick solid line in Figure 10a. Similarly as for PtRu/Vulcan, the adsorbate layer does not inhibit incomplete acetaldehyde oxidation to acetic acid at potentials negative of the onset of CO_2 formation.

Steady-state currents for acetaldehyde oxidation on the Pt_3Sn/Vulcan electrode were evaluated in a potential-step transient measurement (0.06–0.61 V). Figure 4 illustrates the evolution of the Faradaic current (Figure 4(d)), of the MS signal for $m/z = 22$ (Figure 4(e)), and of the CO_2 current efficiency (Figure 4(f)). After passing through the initial spike, both the Faradaic current and the CO_2 formation rate decrease slowly over the next 10 min, reaching quasi steady-state conditions with a Faradaic current of 0.005 mA cm^{-2} after 10–15 min. The current efficiency for CO_2 formation is around 2%, which is significantly less than that on Pt/Vulcan, but still double of that on PtRu/Vulcan (see Table 1).

Faradaic current and $m/z = 22$ mass spectrometric current transients, recorded on Pt_3Sn/Vulcan after switching from pure supporting electrolyte to 0.1 M acetaldehyde containing solution, are shown in Figure 5e and f. Both the anodic spike current density and the steady-state current density increase when going to more positive reaction potentials. The quasi steady-state Faradaic current densities for acetaldehyde oxidation obtained after 15 min reaction are 0.006 mA cm^{-2} at 0.51 V and 0.012 mA cm^{-2} at 0.61 V, respectively. The value at 0.61 V is of comparable magnitude to that on Pt/Vulcan, while that at 0.51 V is significantly higher. As discussed previously for the PtRu/Vulcan catalyst (see Section 3.2) we attribute this to the higher activity of the Pt_3Sn for oxidation of C1 decomposition products at lower potentials compared to Pt/Vulcan. The electrolyte exchange transients (Figure 5(e, f)) confirm the result obtained from the potential step measurements that on Pt_3Sn/Vulcan acetaldehyde oxidation is also dominated by incomplete oxidation to acetic acid.

The acetaldehyde adsorbate stripping behavior is shown in Figure 6(e,f), using freshly prepared thin-film electrodes for each experiment. The Faradaic current increases steadily from 0.26 V on, with little difference for the two different reaction potentials, 0.51 V and 0.61 V. Acetaldehyde adsorbate stripping exhibits two regions, a low potential region with a maximum at 0.8 V (onset at about 0.4 V) which is attributed to oxidation of CO_{ad} and partly also $CH_{x,\,ad}$, and a high potential regime (> 0.9 V) which is assigned to oxidation of $CH_{x,\,ad}$ and C2 traces (for discussion see Section 3.1). The relative coverage of C1 species on the Pt_3Sn/Vulcan catalyst is ca. 0.7 for both potentials, i.e., significantly higher than on the PtRu/Vulcan catalyst.

4. Conclusions

Quantitative DEMS measurements of the oxidation of acetaldehyde on carbon supported Pt/Vulcan, PtRu/Vulcan and Pt_3Sn/Vulcan catalyst electrodes and, for comparison, on polycrystalline Pt and on an unsupported $PtRu_{0.2}$ (Adams-type) catalyst electrode, revealed that under present reaction conditions complete oxidation to CO_2 is negligible, being of the order of a few percent; leaving acetic acid as main product. At room temperature acetic acid cannot be further oxidized. CO_2 is produced by oxidation of adsorbed decomposition products resulting from dissociative adsorption. At 0.51 V the activity for acetaldehyde oxidation increases in the order PtRu/Vulcan > Pt_3Sn/Vulcan > Pt/Vulcan (at 0.61 V: Pt_3Sn/Vulcan $\approx$ PtRu/Vulcan < Pt/Vulcan). The results underline that on all catalysts investigated C–C bond breaking is negligible under these reaction conditions.

For Direct Oxidation Fuel Cell applications, the results indicate that for operation at room temperature acetaldehyde oxidation is dominated by incomplete oxidation to acetic acid, while CO_2 formation contributes only with a few percent. The low activity for C–C bond breaking, which is also characteristic for ethanol oxidation, governs acetaldehyde oxidation. Therefore these catalysts will not be able to correct the low selectivities for complete ethanol oxidation observed previously by subsequent complete oxidation of the incomplete oxidation products acetaldehyde and acetic acid. Among the catalysts investigated here the PtRu catalyst may be the most promising one since, based on these and previous results, it has by far the highest selectivity and current efficiency for CO_2 formation at technically relevant low potentials. At these potentials, however, the activity is far too low for applications. Further studies at elevated temperatures are required to elucidate the role of thermal activation on the activity for C–C bond breaking and hence on the selectivity for CO_2 formation.

Acknowledgements

We acknowledge financial support by the Landesstiftung Baden-Württemberg (programme 'Mini Fuel Cells') and by the Deutsche Forschungsgemeinschaft (project Be 1201/12–1). We are grateful to E-Tek, Inc. for the donation of the carbon supported Pt/Vulcan, PtRu/Vulcan and Pt_3Sn/Vulcan catalyst samples and to the Center for Solar Energy and Hydrogen Research (ZSW) for the unsupported $PtRu_{0.2}$ catalyst.

References

1. A.K. Shukla, P.A. Christensen, A. Hamnett and M.P. Hogarth, *J. Power Sour.* **55** (1995) 87.
2. X. Ren, M. Wilson and S. Gottesfeld, *J. Electrochem. Soc.* **143** (1996) L12.
3. C. Lamy, E.M. Belgsir and J.-M. Léger, *J. Appl. Electrochem.* **31** (2001) 799.

4. H. Wang, Z. Jusys and R.J. Behm, *J. Phys. Chem. B* **108** (2004) 19413.
5. B.I. Podlovchenko, O.A. Petry, A.N. Frumkin and H. Lal, *J. Electroanal. Chem.* **11** (1966) 12.
6. M. Shibata and S. Motoo, *J. Electroanal. Chem.* **187** (1985) 151.
7. B. Bittins-Cattaneo, S. Wilhelm, E. Cattaneo, H.W. Buschmann and W. Vielstich, *Ber Bunsenges Phys. Chem.* **92** (1988) 1210.
8. L.-W.H. Leung, S.-C. Chang and M.J. Weaver, *J. Electroanal. Chem.* **266** (1989) 317.
9. B. Rasch and T. Iwasita, *Electrochim. Acta* **35** (1990) 989.
10. S.-C. Chang, L.-W.H. Leung and M.J. Weaver, *J. Phys. Chem.* **94** (1989) 6013.
11. F. Cases, J.L. Vazquez, J.M. Perez, A. Aldaz and J. Clavilier, *J. Electroanal. Chem.* **281** (1990) 283.
12. J.L. Rodríguez, E. Pastor, X.H. Xia and T. Iwasita, *Langmuir* **16** (2000) 5479.
13. E. Mendéz, J.L. Rodriguez, M.C. Arévalo and E. Pastor, *Langmuir* **18** (2002) 763.
14. J. Silva-Chong, E. Méndez, J.L. Rodriguez, M.C. Arévalo and E. Pastor, *Electrochim. Acta* **47** (2003) 1441.
15. K.B. Kokoh, F. Hahn, E.M. Belgsir, C. Lamy, A.R. de Andrade, P. Olivi, A.J. Motheo and G. Tremiliosi-Filho, *Electrochim. Acta* **49** (2004) 2077.
16. H. Wang, Z. Jusys and R.J. Behm, *Fuel Cells* **4** (2004) 113.
17. H. Wang, Z. Jusys, and R.J. Behm, *J Power Sour.* **154** (2006) 351.
18. T.J. Schmidt, H.A. Gasteiger, G.D. Stäb, P.M. Urban, D.M. Kolb and R.J. Behm, *J. Electrochem. Soc.* **145** (1998) 2354.
19. T.J. Schmidt, H.A. Gasteiger and R.J. Behm, *J. Electrochem. Soc.* **146** (1999) 1296.
20. Z. Jusys and R.J. Behm, *J. Phys. Chem. B* **105** (2001) 10874.
21. Z. Jusys, J. Kaiser and R.J. Behm, *Phys. Chem. Chem. Phys.* **3** (2001) 4650.
22. H. Wang, Z. Zhao, Z. Jusys and R.J. Behm, *J. Power Sour.*, **155** (2006) 33.
23. R. Adams and R.L. Schriner, *J. Am. Chem. Soc.* **45** (1923) 2171.
24. K. Lasch, L. Jörissen and J. Garche, *J. Power Sour.* **84** (1999) 225.
25. H. Baltruschat, 1999, *in* A. Wieckowski (Ed), 'Differential Electrochemical Mass Spectrometry as a Tool for Interfacial Studies in Interfacial Electrochemistry – Theory, Experiment and Applications' (Marcel Dekker, Inc., New York, 1999) pp. 577–597.
26. Z Jusys, H Massong and H Baltruschat, *J. Electrochem. Soc.* **146** (1999) 1093.
27. O. Wolter and J. Heitbaum, *Ber. Bunsenges Phys. Chem.* **88** (1984) 6.
28. H. Baltruschat and U. Schmiemann, *Ber Bunsenges Phys. Chem.* **97** (1993) 452.
29. H. Angerstein-Kozlowska, B.E. Conway and W.B.A. Sharp, *J. Electroanal. Chem.* **43** (1973) 9.
30. H. Wang, Ch. Wingender, H. Baltruschat, M. Lopez and M.T. Reetz, *J. Electroanal. Chem.* **509** (2001) 163.
31. Z. Jusys, J. Kaiser and R.J. Behm, *Langmuir* **19** (2003) 6759.
32. M. Watanabe and S. Motoo, *J. Electroanal. Chem.* **60** (1975) 267.
33. M. Watanabe, M. Uchida and S. Motoo, *J. Electroanal. Chem.* **229** (1987) 395.
34. W.-F. Lin, M.S. Zei, M. Eiswirth, G Ertl, T. Iwasita and W. Vielstich, *J. Phys. Chem. B* **103** (1999) 6968.
35. Z. Jusys, J. Kaiser and R.J. Behm, *Electrochim. Acta* **47** (2002) 3693.
36. T.J. Schmidt, H.A. Gasteiger and R.J. Behm, *J. New Mat. Electrochem. Syst.* **2** (1999) 27.
37. A.C. Boucher, N. Alonso-Vante, F. Dassenoy and W. Vogel, *Langmuir* **19** (2003) 10885.